TECHNICAL MEMORANDUMS

NATIONAL ADVISORY COMMITTEE FOR AERONAUTICS

No. 890

EXPERIMENTS ON A SLOTTED WING

By P. Ruden

Deutsche Luftfahrtforschung
Jahrbuch 1937
Verlag von R. Oldenbourg, München und Berlin

Washington
March 1939

TECHNICAL MEMORANDUM NO. 890

EXPERIMENTS ON A SLOTTED WING*

By P. Ruden

The results of pressure distribution measurements
that were made on a model wing section of a Fieseler F 5 R
type airplane are presented in this report. Comparison of
these model tests with the corresponding flight tests in-
dicates the limitations and also the advantages of wind
tunnel investigations, the advantages being particularly
that through the variety of measuring methods employed
the more complicated flow conditions may also be clarified.
A fact brought out in these tests is that even in the case
of "well rounded" slots it is possible for a vortex to be
set up at the slot entrance and this vortex is responsible
for certain irregularities in the pressure distribution and
in the efficiency of the slot.

I. INTRODUCTION

The tests were conducted at the instigation of the
DVL, which for its part carried out pressure-distribution
measurements in flight on a wing section of the Fieseler
F 5 R type airplane. By parallel tests in the wind tunnel
it was intended to obtain new data on the question of the
applicability of wind-tunnel measurements to full-scale
conditions. In addition, wind-tunnel investigations ap-
peared particularly well suited to clarify the flow phe-
nomena in the wing slot. The interpretation of the pres-
sure-distribution measurements, however, although supple-
mented by boundary-layer investigations, was so difficult
that it was necessary to render the flow visible. The
simplest method that at first suggested itself was that of
observing the water flow in an open channel in which a
wooden model of the slotted wing was placed. Unfortumate-
ly, this method proved quite inadequate, since, in order
to maintain the Reynolds Number as large as possible,
higher flow speeds were required than those normally em-
ployed. With such high speeds, however, the disturbances

---

*Versuche an einem Düsenflügel." Jahrbuch 1937 der deutschen
Luftfahrtforschung, pp. I 75-86.

due to the surface waves in the slot become so strong that
the surface condition no longer reflects the true picture
of the corresponding air flow. Reliable results can be ob-
tained only by means of underwater-flow pictures, although
in this case it is not quite possible to attain the Reynolds
Number of the wind-tunnel tests, because of illumination
difficulties encountered.

II. PROCEDURE IN WIND-TUNNEL TESTS

Since the primary object of the wind-tunnel investiga-
tions was the comparison with the DVL flight tests, the
pressure-distribution measurements were made on a model
wing of the Fieseler F 5 R type airplane already mentioned,
only the left half-wing reduced to the scale 1:5 being
employed. This half-wing could be mounted as a cantilever
wing on a rotating circular end plate of plywood with the
prescribed dihedral in the free jet of the tunnel (fig. 1).
The wing section at which the pressure distribution was
measured with the aid of pressure orifices was the same as
that employed in the DVL flight tests. The profile section
is shown in figure 2, the hinge axis of the flap being in-
dicated. Figure 2 likewise shows the position of the pres-
sure orifices. Although an attempt was made to obtain a
large number of pressure orifices in the slot, it was not
possible for lack of space to bore orifices in the neigh-
borhood of the flap nose. For the same reason, it was nec-
essary to dispense with an orifice on the upper surface at
the trailing edge of the main wing.

The tests were conducted at a wind velocity of 34.8
m/s (78 m.p.h.). The Reynolds Number based on the chord
of the section t = 292.8 mm was about 7×10^5. The ai-
leron always remained in the undeflected position, the
flap setting β and the angle of attack α being varied.
The angle α is the geometric angle of attack (without
wind-tunnel correction) taken with respect to the direc-
tion of the reference axis (fig. 2). The flap settings
were taken to be $\beta = 0°$, $10°$, $19°$, and $34°$. (In the DVL
measurements, the settings were $0°$, $19°$, and $32°$.)

The angle-of-attack range investigated embraced the
two separation ranges. Since it was first assumed that
within the range of "adhering flow" the pressure curve
taken as a function of the angle of attack at any measur-
ing point would show no irregularities, the relatively

large angle-of-attack interval of about 6° was chosen and
this was reduced to about half only in the neighborhood
of the separation ranges. On evaluating the results, it
was found, however, that the expectations entertained with
regard to the smoothness of the pressure curves were in no
way fulfilled. In order to check this result, subsequent
measurements were made at β = 34° for additional angles
of attack.

The extrapolation of the pressure-distribution curves
from pressure orifice 9 down to the trailing edge of the
main wing presents great uncertainty. For this reason,
pressure measurements for several combinations of α and
β were made along the upper surface of the main wing down
to the trailing edge with the aid of a fine static tube.
At those positions where the surface pressures could be
determined in the usual manner, the reliability of this
method could be checked by comparison. It turned out, as
was also expected, that the measuring accuracy of the
static tube in the immediate neighborhood of the wing sur-
face was unsatisfactory, but nevertheless did give a cor-
rect indication of the general tendency of the pressure
diagram.

Finally, with the aid of a fine Brabbée tube of about
0.8 mm outside diameter, the distribution of total pres-
sures was measured in a normal section close behind the
slot outlet for a flap setting of 34°. Since the wing
changes its attitude somewhat with the wind on as compared
with its attitude in quiet air it was necessary for the
distance of the tube from the wing to be determined during
the measurement itself. This could be done in a relatively
simple manner by determining the position of smallest total
pressure behind the main wing trailing edge with the great-
est possible accuracy. Before each measurement the total
pressure tube was adjusted to the mean flow direction with
the aid of a streamer. Since with fixed angle of attack
and flap deflection, appreciable changes in flow directions
are not likely to arise within the boundary layer and the
slot and since the Brabbée tube is very insensitive to
changes in direction, this method of adjusting the total
pressure tube in the flow direction appeared sufficiently
accurate. Check tests with somewhat varied tube directions
showed in fact that the measurements were excellently re-
producible.

III. PRESSURE DISTRIBUTIONS

The results of the pressure-distribution measurements
are contained in tables 1 to 4. The pressures at the sur-
face are expressed in fractions of the dynamic pressure   q
corresponding to the tunnel velocity. The intermediate
measurements mentioned above are not indicated. Figures 3
to 6 show as examples the pressure distribution diagrams
for $\beta = 0°$ and $\beta = 34°$ plotted against the reference
axis of the wing section. For $\beta = 34°$ the plots are pre-
sented in such a manner as if the flap were rotated back-
ward from its zero position, this manner of presentation
adding to the clearness of the diagram.

The pressure-distribution curves shown are generally
somewhat uncertain at their sharpest maxima since no meas-
urements were actually made at the corresponding positions.
Thus, for example, the peak on the upper surface at the
wing leading edge is seldom accurately known, although it
is just in this region that the orifices are most closely
spaced. On the upper surface of the main wing similar
difficulties are encountered in the neighborhood of the
trailing edge, particularly since space limitation pre-
vented installation of a pressure orifice here.

For $\beta = 0°$ the entire appearance of the pressure-
distribution curve indicates that at this position, the
pressure on the suction side of the main wing passes over
smoothly into the pressure at the suction side of the flap.
This would also follow from the fact that the slot outlet
is nearly closed for $\beta = 0°$. For greater flap settings,
this, however, is no longer the case. The fact that the
dotted peaks arise in this case was already shown by the
above-mentioned qualitative measurements with the static
tube.

For $\beta = 0°$ the slot, as mentioned above, was almost
closed. In the pressure distribution this shows up in the
value the pressure assumes in the entire slot, the value
being that which is attained at the lower side of the sec-
tion at the inlet to the slot, and in the discontinuous
change which the pressure undergoes both on the upper side
of the flap as well as at the trailing edge of the main
wing in the passage through the slot outlet. This discon-
tinuity is indicated in the pressure-distribution curves
(figs. 3 and 4) by the two closely lying vertical lines.
At the lower left edge of these vertical lines, the pres-

sure curves include a doubly enclosed region, which does not, however, contribute anything in the integration, since it must be traversed once in one direction and then in the reverse direction. If this doubly enclosed region is neglected, the pressure distribution for $\alpha > 7.6°$ barely differs from those of a corresponding simple section. In the case of small negative angles of attack, however, there is a definite disturbance on the lower surface, which shows up in the fact that there is a greater pressure rise at the leading edge of the flap on the upper surface than on the lower surface.

As examples of the pressure-distribution diagrams that are obtained with open slot, there are shown the pressure-distribution curves for $\beta = 34°$ (figs. 5 and 6). The characteristic phenomena show up most clearly in this case. For large negative angles of attack, the flap lies almost completely in the wake region of the main wing. The flap pressure distribution is correspondingly distorted. Since the air which flows past the flap consists of the small energy content boundary layer, the full dynamic pressure $(p/q = 1)$ is not attained at the stagnation point, which, on account of the division of the flow, must necessarily lie in the neighborhood of the flap nose. This pressure is first attained for $\alpha > -7.4°$. The maximum pressure on the flap upper surface at first rapidly increases with increasing α up to $\alpha = 1.6°$ and then drops again to a constant value between $\alpha = 7.6°$ and $16.7°$. In the angle-of-attack range $1.6° \leq \alpha \leq 16.7°$, the pressure rise along the upper surface of the flap is satisfactory. At $\alpha = 19.7°$, the maximum negative pressure on the upper surface of the flap drops rather abruptly. The flow separates and thereby initiates separation also on the upper surface of the main wing. The pressure changes here described can be conveniently followed with the aid of figure 7 where the pressures at each of the pressure orifices have been plotted as functions of the angle of attack. The most important result established is the following: For a given flap setting and given dynamic pressure corresponding to the tunnel velocity, the largest negative pressures at the flap nose occur at a small angle of attack, corresponding to high-speed flight. The flap nose may thus, under certain circumstances, experience unusually high stresses.

IV. THE FLOW PAST THE SLOT

Considered from the physical point of view, the lower-
ing of the negative pressure peaks on the upper surface
of the flap in the angle-of-attack range $1.6° \leq \alpha \leq 7.6°$
is particularly striking. Considering the pressures at
orifices 10 to 13 lying at the slot inlet on the under sur-
face of the main wing, there is an even more remarkable
sudden change observed in the above-mentioned angle-of-at-
tack range. Whereas, for $\alpha = 1.6°$ at the slot side of
the main wing, an initial drop in pressure is followed by
a rather strong pressure rise (fig. 5), for $\alpha = 7.6°$,
these pressure fluctuations no longer occur (fig. 5). The
reason for the pressure changes indicated above for $\alpha =
1.6°$ becomes clear if it is assumed that a vortex is built
up at the slot inlet as sketched on figure 12a. Since the
vortex contains only the boundary-layer air, the value
$p/q = 1$ is not attained at the stagnation point behind the
vortex. At larger angle of attack the vortex completely
disappears for $\beta = 34°$.

That quite similar phenomena occur for other flap de-
flections, $\beta = 10°$ and $19°$, is shown by figures 8 and 9.
In these the pressure distribution curves have been col-
lected for all of the values of β investigated (with the
exception of $\beta = 0°$) and for $\alpha = 1.6°$ and $\alpha = 7.6°$.
The only difference that occurs for $\beta = 10°$ and $19°$ as
compared with the case previously discussed for $\beta = 34°$
is in the fact that the slot vortex apparently does not
quite disappear at the higher angles of attack but only
becomes smaller. This may be accounted for by the fact
that the flow through the slot at the smaller flap deflec-
tions is throttled considerably more at the narrow outlet
of the slot than at $\beta = 34°$.

In order to prove the actual existence of the vortex
at the slot inlet, pictures of the flow through the slot
were obtained in a water channel. After several prelimi-
nary tests it was found to be necessary to abandon the
usual method of surface pictures and conduct the tests in
a closed channel having a flow cross section of 250 × 500
mm^2. The model of the slotted wing had a chord of 200 mm
and a span of 250 mm; i.e., it extended from one wall to
the other. The airfoil section was the same along the en-
tire span. The middle plane of the channel was illuminat-
ed with the aid of two arc lamps the paths of whose rays
were concentrated on the plane by cylindrical lenses,

Particles that were suspended in the water ahead of the
model wing reflected the light in this plane and traced
the flow paths. Since with the existing illumination ap-
paratus, it was necessary to employ particles with as good
reflecting ability as possible, aluminum powder that was
usually used in the surface pictures was again employed.
The difficulty of making the aluminum powder remain sus-
pended under the water was overcome by adding alcohol to
the powder. With this addition, the favorable condition
was simultaneously obtained of reducing the total weight
of the suspended particles to such an extent that a large
part of the aluminum powder could remain suspended in a
water-filled stand cylinder without appreciable sinking
velocity.

The flow through the slot thus rendered visible in
the manner described above was photographed. Particular-
ly beautiful pictures from which quantitative results
could also be also be derived were obtained when a rapid-
ly rotating diaghragm, which broke up the streamline pic-
ture evenly, was mounted in front of the camera objective.
Figure 10 shows one such photograph obtained. In the cor-
responding test the flow velocity of approach was somewhat
above 1 m/s (2.24 m.p.h.), the Reynolds Number referred to
the model chord being about 2×10^5. The model wing pro-
file agreed in outer contour with that shown in figure 2.
The slot inlet, however, even in the preliminary tests was
widened. The vortex at the entrance in this case, even
for the relatively large angle of attack of 4°, is very
clearly shown. The flap deflection was 10°.

In the preliminary tests, which were also conducted
with the slot shape of figure 2, it was found that the
vortex practically disappeared at larger values of α.
The corresponding photographs are unfortunately unsuited
for reproduction.

There is still to be considered the question whether
the vortex occurs also at larger Reynolds Numbers. For
the Reynolds Number of the wind tunnel its existence is
assured by the measured pressure distribution. Whether
it exists at much higher Reynolds Number can only be es-
tablished by further tests.

In order to investigate somewhat more closely the
effect of the vortex on the flow past the slot, total pres-
sure measurements were made close behind the slot exit dur-
ing the wind-tunnel tests on the model wing of the F 5 R

airplane. The flap setting β was again 34°. Figure 11
shows the results of this investigation. The height of
the total pressure peak suffers the same fluctuations as
the negative pressure peak of the flap upper surface. At
large negative angles of attack the energy of the flow
through the slot is small. The loss is a result of the
adverse pressure gradient, which the boundary layer at the
under side of the section must overcome in its path from
the main wing nose to the slot inlet (see fig. 5, α =
-13.5° to -4.4°). With increasing angle of attack the ad-
verse pressure gradient becomes smaller and the total
pressure maximum at the slot exit as well as the negative
pressure peak at the flap upper surface increase in height
in about the same ratio in which the pressure gradient de-
creases. Simultaneously the vortex at the slot inlet is
built up as shown by the pressure distribution at the in-
let. In a remarkable manner the total pressure and nega-
tive pressure peaks attain their maximum values precisely
when the pressure distribution curves indicate the most
marked formation of the vortex, namely at the angle of at-
tack $\alpha = 3^\circ$. With increasing angle of attack the height
of the total pressure peak decreases very rapidly and then
slowly again increases. The negative pressure peak on the
flap upper surface also begins to decrease immediately
above $\alpha = 3^\circ$ but does not increase again after that.
Figure 11 ($\alpha = 4.3^\circ$ to 16.3°) provides a simple explantion
for this. The boundary layer from the main wing upper
surface increases in thickness with increasing α, so
that the energy transported to the slot is still just suf-
ficient to hold the negative pressure and the stream de-
flection connected with it to a constant height. After
the boundary-layer thickness has exceeded a certain value
(at $\alpha = 17^\circ$) the energy of the slot flow is no longer
sufficient to prevent separation. It is not yet possible
to predict how great this thickness must be for a given
profile section and given energy of slot flow. The deter-
mination of this critical boundary layer-thickness is an
urgent problem in slotted-wing investigation.

The lowering of the total pressure peak in the slot
outlet above $\alpha = 3^\circ$ is evidently connected with the van-
ishing of the slot vortex. It might be expected that with
the disappearance of the vortex there will necessarily be
a considerable increase in the energy of the slot flow, more
particularly since the boundary layer on the under surface
of the main wing has only a small pressure gradient to over-
come, but on the contrary with increasing angle of attack
undergoes stronger accelerations. The measurements show

the contrary to be true, however, at least for the angle
of attack range immediately above 3°. The explanation of
this apparent contradiction probably lies in the stabiliz-
ing effect the centrifugal forces are known to have in
the neighborhood of a convex wall (reference 1). As may
be seen from figure 12, the curvature of the streamlines
at the slot inlet is much greater in the presence of a
vortex than when it is absent. Correspondingly the cen-
trifugal effects in the first case are much greater than
in the second.

Fluid particles from the boundary layer and therefore
possessing widely varying absolute velocities are also
acted upon by centrifugal forces of various magnitudes for
streamlines of approximately equal curvature, the slower
particles by smaller, and the faster particles by larger
forces. The former may in a given case be drawn into the
vortex toward the region of lower pressure directed inward.
This action delays turbulent mixing of the boundary-layer
particles with the flow process, which is always associated
with energy losses. At the second curvature of the stream-
lines behind the vortex stagnation point S, the veloci-
ties and hence also the centrifugal forces are small on ac-
count of the nearness to the stagnation point. The stream-
line curvature at this position would tend to promote the
mixing, as may be seen after some consideration but for the
reasons given, however, can have no important effect on the
mixing, particularly since the slowest particles have al-
ready wandered off into the vortex region. The effect of
this centrifugal action is clearly brought out in the form
of the total pressure peaks for $\alpha = -1.9°$ to $+3°$ in fig-
ure 11. The turbulent mixing is so slight that the shape
of the boundary layer of the lower surface may be recog-
nized only at the slot outlet. After the vortex vanishes,
the curvature of the streamlines at the slot inlet becomes
less. At the same time the velocities decrease on account
of the increasing opposing pressure gradient. The result
is that the stabilizing effect of the centrifugal force at
this position becomes too weak to prevent turbulent mixing.
On the other hand, no stagnation point is built up within
the slot at the position of second curvature previously
mentioned, so that the centrifugal effects on account of
the high flow velocities occuring there become greater and
may support the turbulent mixing. This is shown both in
the shape and in the height of the toal pressure peaks for
$\alpha \geq 3.7°$.

The explanation here given of the slot flow has not

gone into a thorough description of the processes involved.
It was nevertheless presented with sufficient detail, since
it appeared important to show clearly with the aid of an
example the many aspects of the problems connected with the
slotted wing and thus provide starting points for the indis-
pensable detail investigations. The fact that even for
slots given as "well rounded" a vortex is set up at the en-
trance is not only interesting in itself but will lead to a
study of what shape the slot should be given in order that
such a vortex formation may be avoided. As is shown on fig-
ure 10, a flattening of the slot inlet should have no favor-
able effect. On the contrary, a slot inlet of still greater
curvature as shown in figure 2 should be better. It is to
be observed that the shape of a good slot inlet certainly
depends also on the width of the slot at the exit and hence
on the amount of throttling. Since there is a steady flow
of new air from the boundary layer to the vortex, there
must necessarily occur a throwing off of vortex material.
With this process are associated periodic pressure fluctua-
tions. Their frequency appears to lie so high, however,
that they are not likely to give rise to flutter. It is
possible, however, that the undesirable vibrations of the
ailerons, which are sometimes observed with slotted wings,
may be connected with these frequencies. No systematic ex-
planation has as yet been given of the question as to what
extent the flow resistance through the slot is affected by
the vortex formation. In the treatment of all these ques-
tions, there must also naturally be taken into account the
questions of control surface balance.

V. THE SEPARATION PROCESS

For the sake of completeness of the discussion of the
pressure-distribution curves, there will be given a short
description of the separation process. The highest measured
negative pressure peaks in the neighborhood of the nose of
the airfoil are given in table 5. The absolute numerical
values increase with β (except for $\beta = 34°$). They show
clearly how the upper surface boundary layer is made capable
of overcoming a large pressure gradient through the energy
in the slot, which increases with β.

Table 5

β	$(p/q)_{min}$
$0°$	-4.40
$10°$	-4.70
$19°$	-5.35
$34°$	-5.31

In the separation process, two stages may be recognized:

1. The separation proceeds from the trailing edge of the section forward without, however, reaching the airfoil nose. This shows up in the smaller negative pressures in the separation zone. At the nose a negative pressure peak is maintained.

2. Complete separation of the flow on the upper surface - the negative pressure peaks on the upper surface vanishing.

In the first stage an important difference arises on the one hand for $\beta = 0°$ and $10°$, and on the other hand for $\beta = 19°$ and $34°$. Whereas, in the first case, the separation point shifts rather steadily from the trailing edge forward, in the second case the separation occurs much more violently. At negative angles of attack the two stages in the flow separation are not so clearly discernible.

VI. INTEGRATION OF PRESSURE-DISTRIBUTION CURVES

It will be assumed in what follows that the x and y axes are as indicated in figure 2 and remain fixed to the main wing. When the flap is deflected by an angle β, the x and y coordinates of the pressure orifices which lie on the main airfoil remain unchanged while those on the flap change their coordinates. Plotting the measured pres-

sures against the x and y axes, respectively, the nor-
mal and tangential force coefficients may be determined by
integration. By using the integration, there is at the
same time obtained the pitching-moment coefficient with
respect to the origin of coordinates O (fig. 2). We have

$$c_n = \oint_{1,2} \left(\frac{p}{q}\right) d\left(\frac{x}{t}\right) \qquad c_t = \oint_{1,2} \left(\frac{p}{q}\right) d\left(\frac{y}{t}\right)$$

$$c_m = \oint_{1,2} \left(\frac{p}{q}\right) \left(\frac{x}{t}\right) d\left(\frac{x}{t}\right) + \oint_{1,2} \left(\frac{p}{q}\right) \left(\frac{y}{t}\right) d\left(\frac{y}{t}\right)^*$$

The reference length t is the chord of the wing section,
c_n and c_t are positive in the positive direction of the
y and x axes, respectively, and c_m is positive for a
nose-heavy moment. In the integration, the pressure dis-
tribution of the main airfoil (subscript 1) and that of the
flap (subscript 2) are to be integrated separately. The
accuracy of the coefficients thus obtained depends natural-
ly very much on the reliability with which the points have
been obtained for the corresponding pressure distribution.
The c_t values are therefore relatively uncertain, since

in the plot against y the contour of the nose of the air-
foil becomes of great importance and with the large changes
in pressure occurring at that position the existing number
of pressure orifices is by no means sufficient. The above-
mentioned lack of sufficient information on the pressure
variation at the main airfoil nose shows up to the greatest
extent in the determination of the pitching-moment coeffi-
cient principally in the first integral. The contribution
of the second integral is always relatively small, although
by no means negligible since it may amount to 5 percent of
the value of the first integral. Aside from the above-men-
tioned uncertainties, the values of the coefficients ob-
tained through integration of the pressure distribution
curves cannot fundamentally correspond with those obtained
by force measurements, since the effect of the skin fric-
tion is neglected.

---

*The relation between the coordinates x and y and the
coordinates X and Y indicated in figure 2 is given by

$$X = \frac{x}{t} 100, \qquad Y = \frac{y}{t} 100.$$

The values of the coefficients c_n, c_t, and c_m given by integration of the pressure-distribution curves are given at the heads of tables 1 to 4, and are plotted in figures 13, 14, and 16 as functions of the angle of attack. The curves of c_n against α, except for the stalling ranges, show the usual approximately linear relation. For positive c_n the critical angle of attack at which separation begins becomes smaller as the flap deflection β becomes larger. For negative c_n the reverse is the case. Figure 14 shows how the coefficient c_t becomes unfavorable with increasing β, since the drag becomes greater, the greater the value of c_t becomes. On the c_t curves, moreover, the two stages of separation are clearly evident. The value of c_t increases in two relatively sharp jumps, the first of which, at $\beta = 19^{\circ}$ and 34°, is much greater than that at $\beta = 0^{\circ}$ and 10°. This corresponds to the fact brought out in the previous section that the first stage of the separation process in the case of the first pair of flap deflections sets in much more violently than in the case of the second pair. Figures 13 and 14 also indicate the proportion of the contributions of main airfoil and flap. Particularly striking is the fact that c_{n_2}, the normal force coefficient of the flap, is practically constant. The increasing reduction in c_t with increase in β is brought about exclusively by the flap. In the value of c_{t_2}, the tangential force coefficient of the flap, there also enters (for $\beta = 19^{\circ}$ and 34°) the drag increasing effect of the slot vortex.

From the values of c_n and c_t there were computed (without wind-tunnel correction, however) the values of the lift and drag coefficients c_a and c_w, plotted as polars in figure 15. The increase in drag with increasing flap deflection is particularly evident.

Whereas the processes which may be associated with the appearance of the slot vortex do not show up in the normal force coefficient c_n, they do show up very clearly in the values of c_m (fig. 16). The slope $dc_m/d\alpha$ is noticeably changed in the angle of attack range $3^{\circ} < \alpha < 8^{\circ}$. For $\beta = 34^{\circ}$, the curve c_m is drawn through a particularly large number of test points that were subsequently obtained.

VII. COMPARISON OF WIND TUNNEL MEASUREMENTS

WITH THE RESULTS OF THE FLIGHT TESTS

An entirely satisfactory comparison of both these sets
of measurements is not simple. This is first of all due to
the difficult conditions under which it was necessary to
carry out the flight tests. The number of pressure orifices
could not be made as large as would be necessary for an en-
tirely reliable determination of the pressure distribution.
At the main wing trailing edge from X = 60.0 on, there
were no pressures orifices. In the case of the model wing,
there were in this region the four orifices 9 to 12. In
addition to the difficulty of obtaining an approximately
correct pressure distribution in this region, however,
it was necessary, in evaluating the flight test results, to
fair the curves arbitrarily at these positions, particularly
since the supplementary qualitative measurements with the
static tube that were found useful in the wind tunnel tests
were not available. Moreover, the pressure orifices at the
airfoil nose in the flight tests were not as numerous as in
the wind-tunnel tests. In the DVL tests, the first pressure
orifice was located at X = 2.5, while in the wind-tunnel
test orifice 1 was at X = 0, orifice 2 at X = 2.22, and
orifice 17 at X = 2.56. At the airfoil nose the stagnation
point and the maximum negative pressure position are close
beside each other. With increasing distance from the air-
foil nose, the pressure differences between the upper and
lower surfaces rapidly decrease. It was, therefore, to be
expected that the DVL tests would give smaller resultant
pressures than the model tests. A particular difficulty
encountered was the fact that in the flight tests it was
necessary for practical reasons to connect up the pressure
orifices on the upper and lower surfaces with each other.
If the pressures are measured individually as was the case
in the model tests, the stagnation point at the nose of the
airfoil can be given with relative accuracy if at no pres-
sure orifice the value $p/q = 1$ is attained. For the
method of measurement used in the DVL test, however, this
was not longer possible.

On the other hand, on account of the small dimensions
of the model, the model test had the disadvantage that com-
plete geometric similarity, in spite of all care taken,
could hardly be attained. The slot lip of the model was
particularly difficult to construct, since the main airfoil
trailing edge ends very sharply and for reasons of strength
the model thickness could not go below a certain limit. It

is also very difficult to reproduce the shape of the airfoil nose with the required accuracy when it is considered that it is at this position that the pressure is extremely sensitive to the smallest changes in shape (reference 2).

With the above considerations in mind, no too strict rule should be applied for the comparison of the pressure distributions. Actually, for example, according to figure 17, large differences arise at the airfoil nose at $\beta = 0°$. For comparison, the pressure distributions for the same value of c_n were drawn above each other. The curves of the flight measurement are interpolated from the values given by Kiel (reference 3) while the resultant pressure for the model test had to be read off from the drawn pressure distribution curves. On account of the steep slope of the pressure curves at the airfoil nose, the pressure difference of two points lying above each other is never uniquely determined, since there is a chance for large discrepancies in the measurements. Only for the larger values of x does the determination of the pressure differences become to some extent reliable.

The curves for $\beta = 0°$, $c_n = 0.60$ (fig. 17) are particularly interesting. The stagnation point obviously remains undetermined on the curve corresponding to the flight measurement. In figure 3 for the corresponding pressure-distribution curve $\beta = 0°$, $\alpha = 7.6°$, the test points which would correspond to the first two pressure orifices of the flight measurements are indicated by large crosses. Their position confirms what was said. The same applies to the other curves of figure 17. From the pressure distributions of figure 4 for $\beta = 0°$, $\alpha = 16.7°$ ($c_n = 1.18$) and $\alpha = 19.7°$ ($c_n = 1.26$) there may be determined the resultant pressure which corresponds to the first two pressure orifices of the DVL test and thus show that the stagnation point and maximum negative pressure are both undetermined. At a greater distance from the airfoil nose, the agreement between the wind-tunnel measurement and the flight tests is surprisingly good, although the error made in drawing the pressure distribution curves enters the value of c_n and equal c_n values were chosen as a basis for comparison.

The comparison of the resultant distributions for $\beta = 19°$ also shows quite satisfactory agreement for $c_n = 1.15$, 1.55, 1.80. An exception must here be made naturally for the differences at the airfoil nose for which the explanation may again be found in the measured pressure distributions in the wind tunnel. There may be observed here the additional small peak at the main airfoil trailing edge. The flight test provided no test points for the pressure distribution for this region since, as already mentioned,

there were no pressure orifices at the main airfoil trail-
ing edge. From the comparison of the pressure-difference
curves it was found that the value of c_n given by Kiel is
somewhat too small, since his curves drop too sharply at
the main airfoil trailing edge. The curves of figure 18
show the greatest additional peak for $c_n = 0.75$. For this
reason the agreement of the continuous and dotted curves in
this case is here also the least favorable. If, however,
the value of 0.66 given by Kiel is used, the agreement, ex-
cept for the main wing trailing edge, is again very good.

Figure 19 gives the values obtained by integration of
the flight measurements and the wind-tunnel measurements
for $\beta = 0°$ and $19°$. Even taking into account the fact
that in the case of the model wing the flow separation oc-
curs much earlier than in the full-scale wing, the agree-
ment is nevertheless satisfactory. The fact that the
points with reference to which the pitching-moment coeffi-
cients were obtained were somewhat different is not par-
ticularly important. A recomputation of the wind-tunnel
results using the reference point of the DVL measurements,
which point coincides approximately with orifice 1 (fig. 2)
gives only a slight shift in the values. It will be seen,
however, that the moment coefficients of the flight test
are greater for $\beta = 0°$ and smaller for $\beta = 19°$. It
should be remarked that for $\beta = 19°$ the resultant pres-
sure distributions given by Kiel necessarily yield a smaller
pitching-moment coefficient since the omitted smaller pres-
sure peak at the main airfoil trailing edge exerts an ap-
preciable effect on account of the large lever arm.

Summarizing, it may be stated that the wind-tunnel
tests give quite reliable results in the prestalling range*
but that the separation of the flow occurs much earlier
than in the full-scale tests. If it is assumed that the
maximum value of c_n attained in flight also agrees ap-
proximately with the corresponding value of the wing sec-
tion investigated, the result is obtained that the maximum
normal force coefficient determined in the wind tunnel is
exceeded in flight by 0 to 25 percent (see fig. 20). Aside

---

*It must be expressly emphasized, however, that the devia-
tions in the pressure curves shown in figures 17 and 18 in
the neighborhood of the airfoil nose may, with great prob-
ability, be considered as accidental and further tests are
required for confirmation.

from the fact that the maximum c_n value corresponding to
the measuring section of the flight test is probably higher
than the one here assumed, the comparison given in figure
20 is not entirely free from objection, since in the flight
test the propeller slipstream has a stabilizing effect on
the air flow while in the wind-tunnel test separation of
the flow was promoted by the boundary layer of the end
plate.

VIII. SUMMARY

The results of wind-tunnel tests on a slotted wing are
presented, the object of the investigation being the deter-
mination of the pressure distributions on a wing section
with flap. The model was that of a wing of a Fieseler F5R
type airplane. For studying the flow phenomena in the
slot, total pressure measurements were taken in the boundary
layer behind the slot exit and the flow in the slot of a
similar wing section rendered visible in a water channel.
The attempt to furnish a physical explanation of the slot
flow and its effect on the pressure distribution raises a
number of questions whose answers will have to be provided
by further slotted-wing investigations.

Comparison of the wind-tunnel measurements with the
corresponding flight tests conducted by the DVL showed that
the wind-tunnel results could be reliably applied to full-
scale conditions as long as the below-stalling range is con-
sidered, but that the maximum value of the normal force co-
efficient of the wind-tunnel measurement is from 0 to 25
percent below the value attained in the flight test.

Translation by S. Reiss,
National Advisory Committee
for Aeronautics.

REFERENCES

1. Betz, A.: Über turbulente Reibungsschichten an ge-
      krümmten Wänden. Vorträge aus dem Gebiete der
      Aerodynamik und Verwandter Gebiete, Aachen, 1929,
      pp. 10-18.

2. Betz, A.: Modification of Wing-Section Shape to Assure
      a Predetermined Change in Pressure Distribution.
      T.M. No. 767, N.A.C.A., 1935.

3. Kiel, Georg: Pressure Distribution on a Wing Section
      with Slotted Flap in Free Flight Tests. T. M. No.
      835, N.A.C.A., 1937.

Table 1. Flap deflection $\beta=0°$.

$\alpha°$	$-16,5$	$-13,5$	$-10,4$	$-7,4$	$+1,6$	$+7,6$	$+13,7$	$+16,7$	$+19,7$	$+21,0$	$+22,7$	$+24,6$	$+25,7$
c_n	$-0,67$	$-0,70$	$-0,66$	$-0,49$	$+0,19$	$+0,60$	$+0,99$	$+1,18$	$+1,26$	$+1,33$	$+1,28$	$+1,22$	$+0,92$
c_t	$+0,09$	$+0,07$	0	$-0,02$	$+0,01$	$-0,05$	$-0,16$	$-0,22$	$-0,28$	$-0,29$	$-0,27$	$-0,26$	0
c_m	$-0,25$	$-0,24$	$-0,16$	$-0,11$	$+0,04$	$+0,15$	$+0,25$	$+0,30$	$+0,35$	$+0,39$	$+0,41$	$+0,41$	$+0,33$
Orifice location no.								$\dfrac{p}{q}$					
1	$-0,66$	$-0,68$	$-1,45$	$-1,05$	$+0,85$	$+0,65$	$-0,75$	$-1,87$	$-2,91$	$-3,33$	$-3,52$	$-3,83$	$-0,82$
2	$+0,92$	$+0,89$	$+0,91$	$+0,84$	$+0,04$	$-1,00$	$-2,39$	$-3,17$	$-3,91$	$-4,39$	$-4,38$	$-4,40$	$-0,92$
3	$+0,66$	$+0,60$	$+0,59$	$+0,45$	$-0,38$	$-1,17$	$-2,15$	$-2,67$	$-2,81$	$-2,91$	$-2,72$	$-2,61$	$-0,86$
4	$+0,42$	$+0,35$	$+0,32$	$+0,19$	$-0,57$	$-1,21$	$-1,96$	$-2,29$	$-2,42$	$-2,49$	$-2,24$	$-2,04$	$-0,82$
5	$+0,15$	$+0,09$	$+0,05$	$-0,06$	$-0,69$	$-1,16$	$-1,70$	$-1,85$	$-1,95$	$-1,96$	$-1,65$	$-1,35$	$-0,78$
6	$-0,05$	$-0,10$	$-0,11$	$-0,21$	$-0,67$	$-1,00$	$-1,32$	$-1,46$	$-1,46$	$-1,42$	$-1,05$	$-0,80$	$-0,74$
7	$-0,14$	$-0,16$	$-0,16$	$-0,22$	$-0,55$	$-0,73$	$-0,96$	$-1,02$	$-0,98$	$-0,90$	$-0,70$	$-0,74$	$-0,70$
8	$-0,15$	$-0,15$	$-0,12$	$-0,16$	$-0,37$	$-0,49$	$-0,60$	$-0,61$	$-0,56$	$-0,56$	$-0,70$	$-0,74$	$-0,68$
9	$-0,11$	$-0,09$	$-0,04$	$-0,02$	$-0,14$	$-0,20$	$-0,26$	$-0,24$	$-0,33$	$-0,46$	$-0,65$	$-0,69$	$-0,66$
10	$-0,60$	$-0,49$	$-0,14$	$-0,03$	$+0,15$	$+0,02$	$+0,11$	$+0,16$	$+0,16$	$+0,16$	$+0,15$	$+0,14$	$+0,08$
11	$-0,63$	$-0,50$	$-0,20$	$-0,05$	$+0,11$	$+0,02$	$+0,10$	$+0,15$	$+0,15$	$+0,16$	$+0,15$	$+0,13$	$+0,06$
12	$-0,65$	$-0,55$	$-0,26$	$-0,16$	$-0,05$	$+0,02$	$+0,11$	$+0,16$	$+0,16$	$+0,16$	$+0,15$	$+0,14$	$+0,08$
13	$-0,66$	$-0,62$	$-0,33$	$-0,25$	$-0,10$	$+0,01$	$+0,14$	$+0,19$	$+0,20$	$+0,20$	$+0,20$	$+0,20$	$+0,16$
14	$-0,65$	$-0,84$	$-0,65$	$-0,44$	$-0,16$	$+0,04$	$+0,23$	$+0,32$	$+0,36$	$+0,39$	$+0,40$	$+0,41$	$+0,36$
15	$-0,65$	$-0,89$	$-0,95$	$-0,61$	$-0,21$	$+0,06$	$+0,31$	$+0,42$	$+0,49$	$+0,52$	$+0,54$	$+0,56$	$+0,50$
16	$-0,83$	$-1,00$	$-1,55$	$-1,33$	$-0,38$	$+0,18$	$+0,58$	$+0,73$	$+0,80$	$+0,85$	$+0,85$	$+0,88$	$+0,80$
17	$-1,11$	$-1,21$	$-2,45$	$-2,61$	$-0,35$	$+0,46$	$+0,86$	$+0,92$	$+0,89$	$+0,89$	$+0,85$	$+0,84$	$+0,91$
18	$-0,60$	$-0,47$	$-0,12$	$-0,02$	$+0,15$	$+0,02$	$+0,13$	$+0,17$	$+0,18$	$+0,17$	$+0,17$	$+0,15$	$+0,10$
19	$-0,60$	$-0,48$	$-0,10$	$-0,02$	$+0,17$	$+0,02$	$+0,14$	$+0,18$	$+0,19$	$+0,19$	$+0,18$	$+0,16$	$+0,10$
20	$-0,16$	$-0,10$	0	0	0	$-0,05$	$-0,06$	$-0,06$	$-0,26$	$-0,41$	$-0,55$	$-0,65$	$-0,64$
21	$-0,07$	0	$+0,10$	$+0,12$	$+0,07$	$+0,05$	$+0,03$	$-0,01$	$-0,24$	$-0,39$	$-0,53$	$-0,62$	$-0,60$
22	$-0,12$	0	$+0,13$	$+0,17$	$+0,15$	$+0,14$	$+0,10$	$+0,04$	$-0,21$	$-0,35$	$-0,48$	$-0,58$	$-0,56$
23	$-0,54$	$-0,35$	$-0,09$	$-0,03$	0	$+0,04$	$+0,06$	$+0,05$	$-0,02$	$-0,06$	$-0,14$	$-0,21$	$-0,26$
24	$-0,58$	$-0,40$	$-0,15$	$-0,12$	$-0,09$	$-0,03$	$+0,02$	$+0,04$	$-0,01$	$-0,04$	$-0,09$	$-0,15$	$-0,21$
25	$-0,61$	$-0,45$	$-0,21$	$-0,16$	$-0,10$	0	$+0,07$	$+0,10$	$+0,06$	$+0,05$	$+0,03$	$-0,01$	$-0,06$
26	$-0,62$	$-0,49$	$-0,25$	$-0,21$	$-0,15$	$-0,01$	$+0,08$	$+0,10$	$+0,08$	$+0,08$	$+0,04$	0	$-0,05$

Table 2. Flap deflection $\beta=10°$.

$\alpha°$	$-16,5$	$-13,5$	$-10,4$	$-7,4$	$+1,6$	$+7,6$	$+13,7$	$+16,7$	$+19,7$	$+21,5$	$+22,7$	$+23,6$	$+25,7$
c_n	$-0,50$	$-0,51$	$-0,42$	$-0,16$	$+0,47$	$+0,91$	$+1,29$	$+1,44$	$+1,52$	$+1,52$	$+1,47$	$+1,42$	$+1,02$
c_t	$+0,07$	$+0,04$	$-0,02$	$-0,01$	$+0,02$	$-0,04$	$-0,15$	$-0,22$	$-0,29$	$-0,25$	$-0,26$	$-0,25$	$-0,03$
c_m	$-0,16$	$-0,12$	$+0,01$	$+0,06$	$+0,22$	$+0,31$	$+0,40$	$+0,44$	$+0,49$	$+0,52$	$+0,52$	$+0,51$	$+0,42$
Orifice location no.								$\dfrac{p}{q}$					
1	$-0,55$	$-0,68$	$-1,50$	$-0,70$	$+0,93$	$+0,54$	$-1,12$	$-2,40$	$-3,35$	$-3,70$	$-3,95$	$-3,87$	$-0,62$
2	$+0,94$	$+0,90$	$+0,90$	$+0,79$	$-0,12$	$-1,25$	$-2,74$	$-3,57$	$-4,40$	$-4,62$	$-4,70$	$-4,52$	$-0,75$
3	$+0,65$	$+0,59$	$+0,55$	$+0,39$	$-0,54$	$-1,40$	$-2,41$	$-2,96$	$-2,99$	$-2,94$	$-2,86$	$-2,66$	$-0,75$
4	$+0,40$	$+0,31$	$+0,26$	$+0,10$	$-0,72$	$-1,41$	$-2,19$	$-2,46$	$-2,59$	$-2,46$	$-2,34$	$-2,12$	$-0,73$
5	$+0,11$	$+0,04$	$-0,01$	$-0,16$	$-0,82$	$-1,34$	$-1,87$	$-2,06$	$-2,07$	$-1,88$	$-1,68$	$-1,45$	$-0,71$
6	$-0,09$	$-0,15$	$-0,19$	$-0,30$	$-0,80$	$-1,17$	$-1,50$	$-1,65$	$-1,57$	$-1,29$	$-1,04$	$-0,85$	$-0,69$
7	$-0,20$	$-0,23$	$-0,25$	$-0,32$	$-0,68$	$-0,87$	$-1,11$	$-1,20$	$-1,10$	$-0,84$	$-0,76$	$-0,75$	$-0,67$
8	$-0,23$	$-0,24$	$-0,23$	$-0,27$	$-0,53$	$-0,64$	$-0,75$	$-0,79$	$-0,70$	$-0,71$	$-0,77$	$-0,77$	$-0,66$
9	$-0,25$	$-0,21$	$-0,18$	$-0,20$	$-0,31$	$-0,37$	$-0,42$	$-0,44$	$-0,54$	$-0,69$	$-0,74$	$-0,74$	$-0,67$
10	$-0,54$	$-0,38$	$-0,01$	$+0,10$	$+0,29$	$+0,15$	$+0,26$	$+0,30$	$+0,30$	$+0,30$	$+0,30$	$+0,30$	$+0,27$
11	$-0,51$	$-0,36$	$-0,04$	$+0,05$	$+0,20$	$+0,07$	$+0,16$	$+0,20$	$+0,19$	$+0,18$	$+0,16$	$+0,18$	$+0,14$
12	$-0,61$	$-0,45$	$-0,11$	$-0,05$	0	$+0,12$	$+0,20$	$+0,24$	$+0,21$	$+0,20$	$+0,18$	$+0,19$	$+0,15$
13	$-0,62$	$-0,52$	$-0,20$	$-0,11$	$+0,03$	$+0,14$	$+0,24$	$+0,29$	$+0,28$	$+0,28$	$+0,28$	$+0,28$	$+0,25$
14	$-0,65$	$-0,80$	$-0,50$	$-0,33$	$-0,06$	$+0,14$	$+0,31$	$+0,39$	$+0,41$	$+0,44$	$+0,46$	$+0,46$	$+0,42$
15	$-0,64$	$-0,89$	$-0,76$	$-0,50$	$-0,11$	$+0,15$	$+0,39$	$+0,48$	$+0,54$	$+0,55$	$+0,59$	$+0,59$	$+0,54$
16	$-0,77$	$-1,06$	$-1,45$	$-1,17$	$-0,25$	$+0,28$	$+0,65$	$+0,78$	$+0,84$	$+0,85$	$+0,89$	$+0,89$	$+0,81$
17	$-1,00$	$-1,31$	$-3,08$	$-2,18$	$-0,16$	$+0,59$	$+0,91$	$+0,91$	$+0,86$	$+0,84$	$+0,84$	$+0,83$	$+0,94$
18	$-0,51$	$-0,35$	$-0,01$	$+0,07$	$+0,26$	$+0,14$	$+0,25$	$+0,30$	$+0,30$	$+0,28$	$+0,27$	$+0,29$	$+0,25$
19	$-0,56$	$-0,42$	$-0,29$	$-0,27$	$-0,35$	$-0,31$	$-0,31$	$-0,29$	$-0,44$	$-0,58$	$-0,67$	$-0,67$	$-0,62$
20	$-0,59$	$-0,45$	$-0,35$	$-0,34$	$-0,42$	$-0,35$	$-0,34$	$-0,30$	$-0,46$	$-0,63$	$-0,72$	$-0,73$	$-0,60$
21	$-0,30$	$-0,20$	$-0,11$	$-0,09$	$-0,10$	$-0,09$	$-0,08$	$-0,09$	$-0,32$	$-0,46$	$-0,54$	$-0,58$	$-0,54$
22	$-0,20$	$-0,04$	$+0,07$	$+0,08$	$+0,06$	$-0,01$	0	0	$-0,25$	$-0,41$	$-0,50$	$-0,53$	$-0,50$
23	$-0,46$	$-0,18$	$+0,05$	$+0,08$	$+0,10$	$+0,11$	$+0,15$	$+0,16$	$+0,08$	$+0,02$	$-0,02$	$-0,03$	$-0,06$
24	$-0,52$	$-0,26$	$+0,04$	$+0,09$	$+0,14$	$+0,18$	$+0,22$	$+0,24$	$+0,18$	$+0,15$	$+0,13$	$+0,12$	$+0,09$
25	$-0,55$	$-0,32$	$+0,10$	$+0,23$	$+0,34$	$+0,40$	$+0,44$	$+0,45$	$+0,41$	$+0,40$	$+0,39$	$+0,38$	$+0,36$
26	$-0,55$	$-0,36$	$+0,11$	$+0,31$	$+0,56$	$+0,66$	$+0,70$	$+0,71$	$+0,69$	$+0,68$	$+0,68$	$+0,67$	$+0,66$

Table 3. Flap deflection β=19°.

α^0	−16,5	−13,5	−10,4	−7,4	−4,4	+1,6	+7,6	+13,7	+16,7	+19,7	+21,0	+22,7	+24,4	+25,7
c_n	−0,39	−0,48	−0,22	+0,02	+0,28	+0,75	+1,14	+1,55	+1,74	+1,79	+1,80	+1,20	+1,12	+1,11
c_t	+0,08	+0,04	+0,01	+0,04	+0,06	+0,05	−0,02	−0,14	−0,24	−0,31	−0,32	−0,16	−0,14	+0,05
c_m	−0,09	−0,09	+0,10	+0,18	+0,24	+0,37	+0,45	+0,55	+0,60	+0,62	+0,62	+0,48	+0,48	+0,51
Orifice location no.							$\dfrac{p}{q}$							
1	−0,47	−0,66	−1,43	−0,50	+0,30	+0,94	+0,37	−1,51	−2,92	−4,10	−4,60	−3,15	−3,22	−0,60
2	+0,95	+0,94	+0,91	+0,75	+0,52	−0,27	−1,45	−3,00	−3,99	−5,17	−5,35	−3,94	−3,70	−0,69
3	+0,65	+0,60	+0,55	+0,33	+0,05	−0,66	−1,56	−2,61	−3,12	−3,35	−3,47	−2,05	−1,74	−0,69
4	+0,39	+0,33	+0,25	+0,04	−0,23	−0,85	−1,55	−2,36	−2,69	−2,90	−2,96	−1,38	−0,97	−0,68
5	+0,10	+0,04	−0,04	−0,22	−0,45	−0,94	−1,46	−1,97	−2,25	−2,35	−2,36	−0,60	−0,50	−0,67
6	−0,11	−0,15	−0,22	−0,36	−0,55	−0,91	−1,29	−1,62	−1,81	−1,81	−1,80	−0,51	−0,48	−0,66
7	−0,22	−0,24	−0,28	−0,40	−0,52	−0,80	−1,00	−1,25	−1,36	−1,32	−1,26	−0,52	−0,49	−0,65
8	−0,27	−0,25	−0,26	−0,35	−0,45	−0,66	−0,75	−0,90	−0,96	−0,91	−0,84	−0,55	−0,51	−0,64
9	−0,32	−0,23	−0,22	−0,29	−0,34	−0,46	−0,52	−0,62	−0,65	−0,62	−0,62	−0,57	−0,55	−0,65
10	−0,50	−0,32	+0,08	+0,16	+0,24	+0,36	+0,28	+0,35	+0,40	+0,42	+0,44	+0,35	+0,36	+0,37
11	−0,48	−0,35	+0,05	+0,11	+0,16	+0,28	+0,19	+0,28	+0,33	+0,32	+0,33	+0,25	+0,26	+0,27
12	−0,60	−0,41	+0,03	+0,07	+0,06	+0,09	+0,21	+0,28	+0,33	+0,32	+0,33	+0,25	+0,27	+0,26
13	−0,60	−0,50	−0,09	−0,02	+0,02	+0,13	+0,22	+0,32	+0,37	+0,39	+0,39	+0,33	+0,35	+0,35
14	−0,64	−0,80	−0,40	−0,26	−0,16	+0,02	+0,20	+0,37	+0,45	+0,49	+0,51	+0,47	+0,50	+0,50
15	−0,61	−0,95	−0,64	−0,44	−0,29	−0,03	+0,22	+0,44	+0,54	+0,60	+0,62	+0,58	+0,61	+0,60
16	−0,73	−1,10	−1,42	−1,10	−0,80	−0,14	+0,36	+0,70	+0,82	+0,87	+0,90	+0,86	+0,90	+0,85
17	−0,91	−1,33	−3,05	−1,94	−1,10	0	+0,66	+0,91	+0,90	+0,83	+0,79	+0,85	+0,85	+0,95
18	−0,60	−0,36	−0,16	−0,16	−0,17	−0,13	−0,12	−0,08	−0,04	+0,01	+0,03	−0,07	−0,05	−0,10
19	−0,75	−0,41	−0,39	−0,49	−0,59	−0,75	−0,68	−0,74	−0,69	−0,61	−0,61	−0,79	−0,76	−0,85
20	−0,81	−0,38	−0,39	−0,54	−0,71	−0,92	−0,78	−0,81	−0,72	−0,60	−0,57	−0,80	−0,78	−0,79
21	−0,56	−0,30	−0,17	−0,17	−0,17	−0,22	−0,18	−0,19	−0,19	−0,27	−0,36	−0,50	−0,50	−0,51
22	−0,40	−0,23	−0,15	−0,13	−0,06	+0,01	−0,04	+0,01	+0,01	−0,16	−0,27	−0,42	−0,42	−0,46
23	−0,44	−0,10	+0,10	+0,13	+0,15	+0,20	+0,23	+0,28	+0,30	+0,25	+0,22	+0,10	+0,11	+0,11
24	−0,50	−0,18	+0,23	+0,26	+0,27	+0,32	+0,35	+0,40	+0,44	+0,40	+0,39	+0,30	+0,31	+0,32
25	−0,54	−0,26	+0,34	+0,49	+0,56	+0,60	+0,65	+0,67	+0,69	+0,66	+0,66	+0,61	+0,63	+0,65
26	−0,54	−0,30	+0,25	+0,46	+0,68	+0,90	+0,95	+0,94	+0,95	+0,94	+0,94	+0,91	+0,93	+0,94

Table 4. Flap deflection β=34°.

α^0	−16,5	−13,5	−10,4	−7,4	−4,4	+1,6	+7,6	+13,7	+16,7	+19,7	+20,4	+22,7	+24,4	+25,7
c_n	−0,44	−0,34	+0,16	+0,42	+0,62	+1,14	+1,52	+1,93	+2,11	+2,08	+2,04	+1,29	+1,28	+1,27
c_t	+0,08	+0,09	+0,10	+0,14	+0,15	+0,14	+0,05	−0,07	−0,17	−0,25	−0,26	−0,07	−0,06	+0,13
c_m	−0,12	+0,03	+0,29	+0,39	+0,44	+0,59	+0,65	+0,76	+0,79	+0,77	+0,77	+0,58	+0,57	+0,61
Orifice location no.							$\dfrac{p}{q}$							
1	−0,42	−0,70	−1,05	−0,14	+0,55	+0,91	+0,05	−2,08	−3,65	−4,72	−4,95	−3,20	−3,20	−0,62
2	+0,82	+0,91	+0,85	+0,67	+0,38	−0,50	−1,76	−3,40	−4,71	−5,31	−5,15	−3,75	−3,36	−0,65
3	+0,64	+0,59	+0,46	+0,21	−0,10	−0,87	−1,79	−2,90	−3,30	−3,55	−3,56	−1,88	−1,55	−0,65
4	+0,39	+0,31	+0,16	−0,07	−0,37	−1,04	−1,75	−2,58	−2,95	−3,06	−3,03	−1,19	−0,80	−0,65
5	+0,11	+0,03	−0,12	−0,34	−0,59	−1,11	−1,64	−2,15	−2,46	−2,47	−2,41	−0,54	−0,48	−0,65
6	−0,09	−0,17	−0,30	−0,47	−0,68	−1,09	−1,45	−1,81	−2,00	−1,93	−1,84	−0,50	−0,48	−0,65
7	−0,20	−0,26	−0,37	−0,50	−0,66	−0,96	−1,14	−1,42	−1,55	−1,42	−1,30	−0,50	−0,49	−0,65
8	−0,23	−0,27	−0,37	−0,48	−0,60	−0,84	−0,93	−1,10	−1,17	−1,01	−0,90	−0,52	−0,51	−0,66
9	−0,25	−0,26	−0,37	−0,46	−0,56	−0,71	−0,76	−0,86	−0,92	−0,79	−0,75	−0,56	−0,55	−0,70
10	−0,45	−0,14	+0,24	+0,29	+0,31	+0,42	+0,32	+0,39	+0,43	+0,44	+0,44	+0,40	+0,40	+0,40
11	−0,51	−0,19	+0,19	+0,25	+0,31	+0,40	+0,35	+0,41	+0,45	+0,45	+0,45	+0,42	+0,44	+0,41
12	−0,61	−0,23	+0,20	+0,22	+0,21	+0,24	+0,35	+0,41	+0,45	+0,45	+0,45	+0,43	+0,44	+0,41
13	−0,60	−0,34	+0,12	+0,14	+0,18	+0,28	+0,35	+0,44	+0,49	+0,49	+0,49	+0,45	+0,47	+0,45
14	−0,63	−0,71	−0,21	−0,12	−0,02	+0,14	+0,30	+0,45	+0,53	+0,55	+0,56	+0,53	+0,56	+0,54
15	−0,61	−0,93	−0,43	−0,30	−0,15	+0,09	+0,31	+0,51	+0,60	+0,64	+0,66	+0,62	+0,65	+0,61
16	−0,70	−1,15	−1,19	−0,87	−0,56	+0,03	+0,46	+0,76	+0,85	+0,88	+0,90	+0,86	+0,90	+0,85
17	−0,79	−1,40	−2,52	−1,45	−0,76	+0,20	+0,75	+0,91	+0,85	+0,74	+0,74	+0,83	+0,82	+0,94
18	−0,52	−0,59	−0,95	−1,20	−1,41	−1,73	−1,56	−1,65	−1,65	−1,10	−1,00	−0,91	−0,95	−1,07
19	−0,53	−0,50	−0,95	−1,24	−1,47	−1,85	−1,58	−1,66	−1,65	−0,96	−0,85	−0,89	−0,90	−0,95
20	−0,49	−0,35	−0,60	−0,86	−1,06	−1,50	−1,13	−1,26	−1,31	−0,81	−0,75	−0,81	−0,80	−0,84
21	−0,48	−0,31	−0,35	−0,36	−0,36	−0,32	−0,36	−0,29	−0,27	−0,45	−0,47	−0,51	−0,48	−0,56
22	−0,46	−0,33	−0,32	−0,28	−0,24	−0,12	−0,20	−0,08	0	−0,34	−0,39	−0,41	−0,40	−0,49
23	−0,44	+0,10	+0,30	+0,30	+0,32	+0,40	+0,40	+0,46	+0,50	+0,41	+0,39	+0,35	+0,35	+0,34
24	−0,50	+0,09	+0,56	+0,55	+0,54	+0,59	+0,60	+0,65	+0,66	+0,62	+0,61	+0,58	+0,59	+0,59
25	−0,51	−0,01	+0,58	+0,85	+0,88	+0,88	+0,88	+0,90	+0,90	+0,88	+0,87	+0,86	+0,87	+0,88
26	−0,50	−0,10	+0,31	+0,68	+0,98	+1,00	+1,00	+1,00	+1,00	+0,99	+0,99	+0,99	+1,00	+1,00
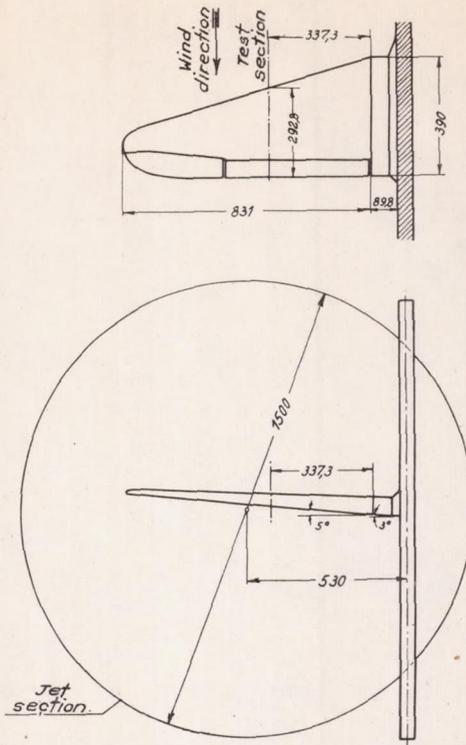
Figure 1.- Arrangement in free jet, plan form and dihedral of model wing.

Orifice location	1	2	3	4	5	6	7	8	9	10	11	12	13	14	15	16	17
x	0	2,22	5,91	9,90	16,50	25,31	36,14	49,36	65,75	71,59	68,95	65,79	56,38	33,07	21,89	7,10	2,56

Orifice location	18	19	20	21	22	23	24	25	26
x	74,05	76,95	79,9	86,10	95,0	90,53	83,13	75,78	72,23
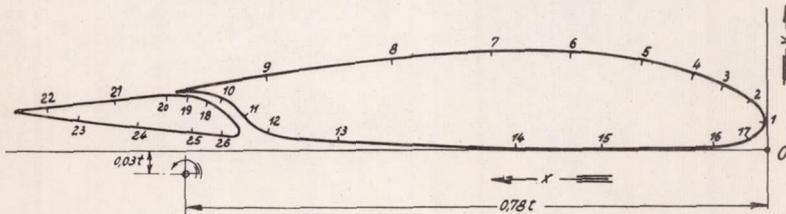
x	0	1,25	2,5	5,0	7,5	10,0	15,0	20,0	25,0	30,0	40,0	50,0	60,0	64,45	66,62	68,65	70,0	71,8	73,8	76,2	77,9	79,67
yo	3,42	5,94	7,07	8,57	9,70	10,52	11,78	12,53	12,98	13,08	12,81	11,81	10,52				9,08					7,65
yu	3,42	1,84	1,37	0,75	0,38	0,14	-0,03	-0,07	0	+0,10	0,44	0,85	1,37	1,60	2,05	3,24	4,44	6,08	7,24	7,68	7,68	7,65

Main airfoil.

x	70,59	70,82	71,80	73,80	76,2	77,9	79,7	80	81,6	90,0	95,0	100,0
yo	2,43	3,11	4,17	5,81	6,93	7,34	7,51		7,38	6,25	5,74	5,40
yu	2,43	2,08	1,98		2,32			2,63		3,72	4,41	5,12

Flap.

Figure 2.- Profile of investigated wing section. Orifices were located at points 1-26.

Figure 4.-
Measured pressure
distributions: $\beta=0°$;
α -16.7° to 25.7°
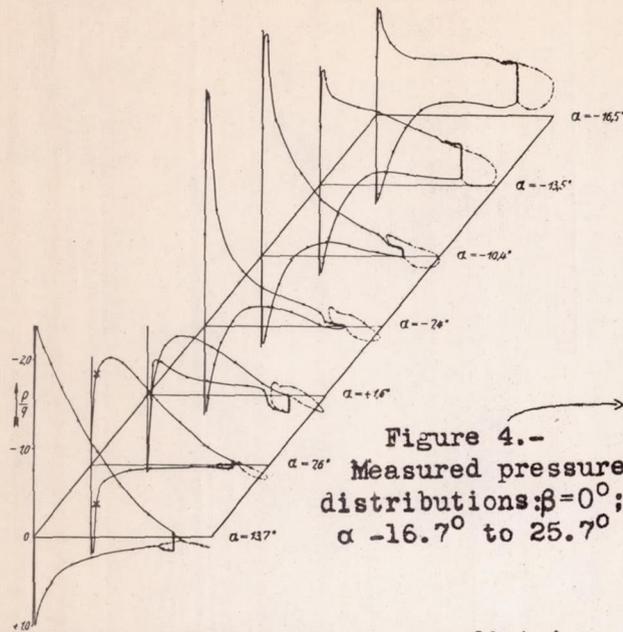
Figure 3.- Measured pressure distri-
butions: $\beta=0°$, $\alpha=-16.5°$ to 13.7°.
The flap pressure distribution is
indicated by dotted line.
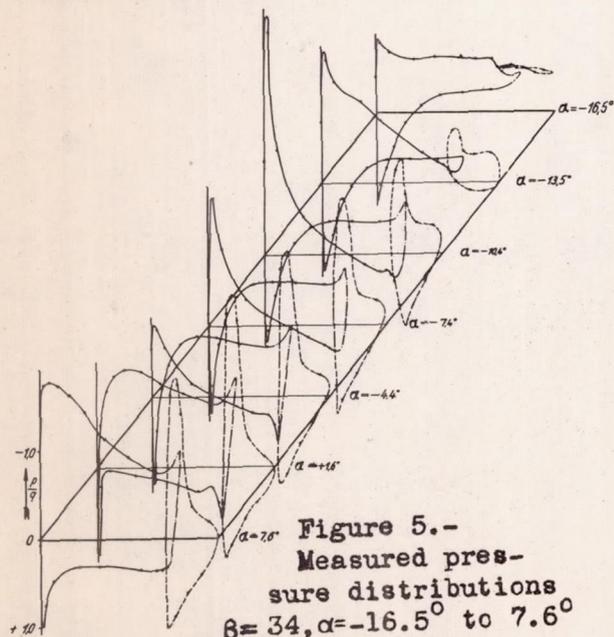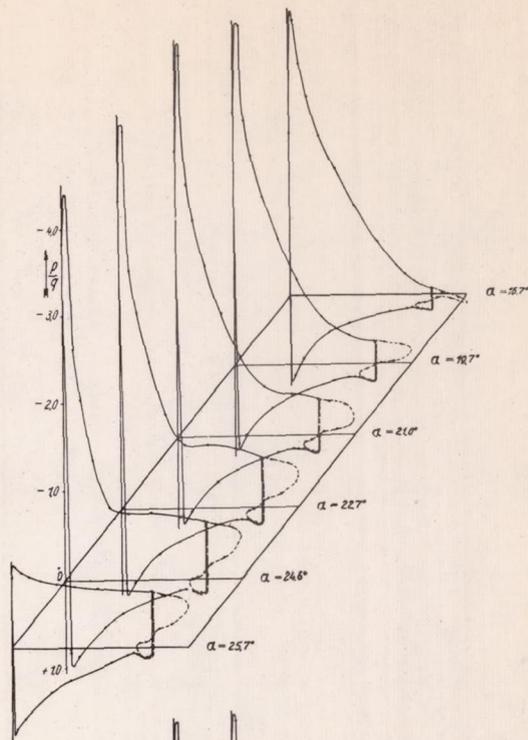
Figure 5.-
Measured pres-
sure distributions
$\beta=34, \alpha=-16.5°$ to 7.6°

The test points of the flap are
so drawn that their distances from
the nose of the section corresponds
to the values given in fig.2.At the
trailing edge of the main wing the
pressure distribution is drawn dot-
ted to indicate that the curve was here
not drawn thru test points and is only
qualitatively correct.
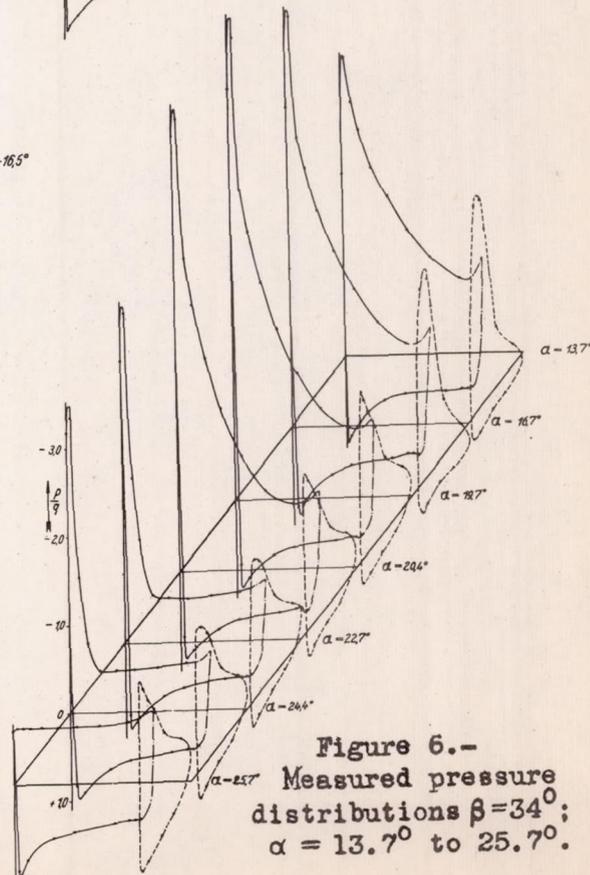
Figure 6.-
Measured pressure
distributions $\beta=34°$;
$\alpha=13.7°$ to 25.7°.
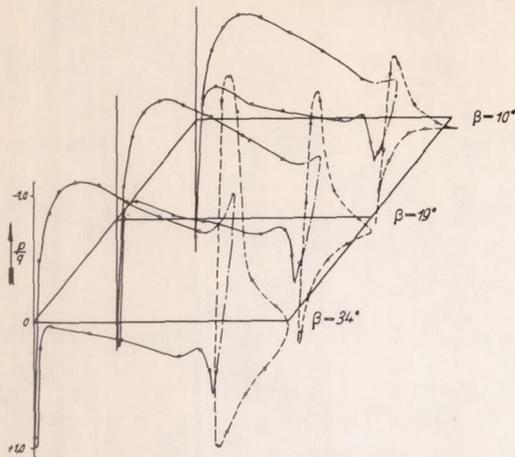
Figure 8.- Measured pressure distri-
butions: $\alpha = 1.6^\circ$
$\beta = 10^\circ$, 19° and 34°.

Figure 7.- Flap pressures for $\beta = 34^\circ$
as functions of α. →
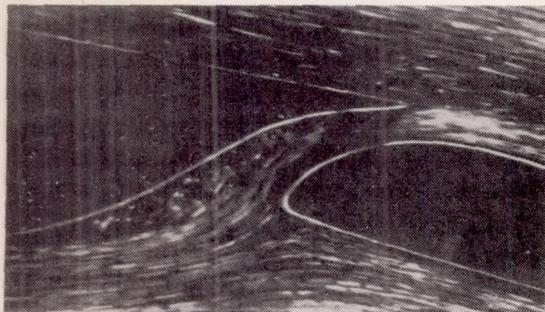
Figure 10.- Stream line picture of slot
flow (flow in closed water
channel), Reynolds Number about 2×10^5.
Slot inlet is somewhat widened as com-
pared with that of fig.2, $\alpha = 4^\circ$, $\beta = 10^\circ$.

Orifice location		
"	18	○
"	19	●
"	20	◎
"	21	◉
"	22	⋈
"	23	●
"	24	+
"	25	○
"	26	✦
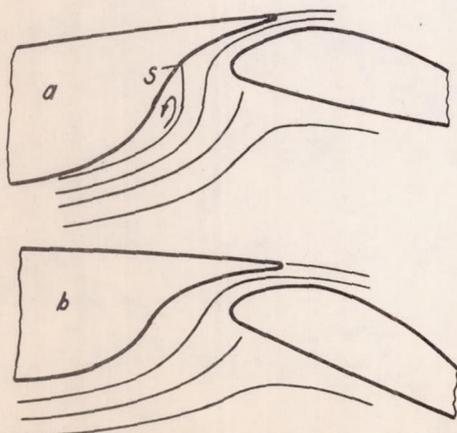
Figure 12.- Sketch of slot flow,a for
$\alpha < 3^\circ$, b for $\alpha > 5^\circ$. Flap setting 34°.
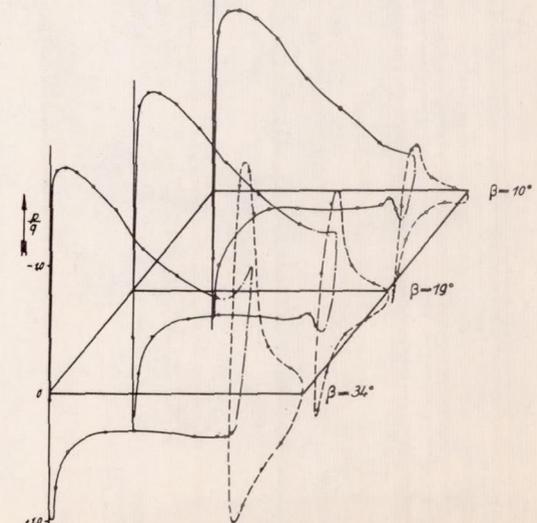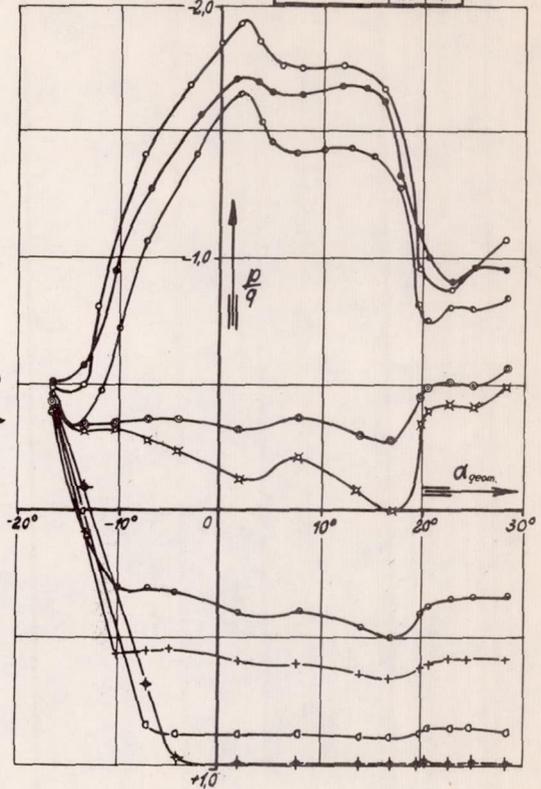
Figure 9.- Measured pressure dis-
tributions: $\alpha = 7.6^\circ$, $\beta = 10^\circ$, 19°
and 34°.

Figure 11.- Total pressure measure-
ments at slot exit
for a flap deflection β=34°.

Fig. 11
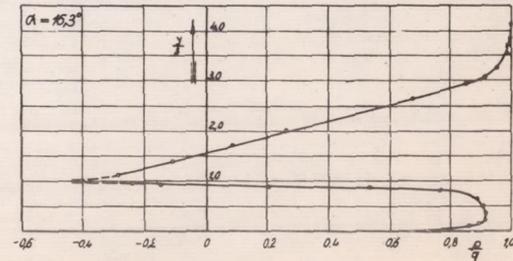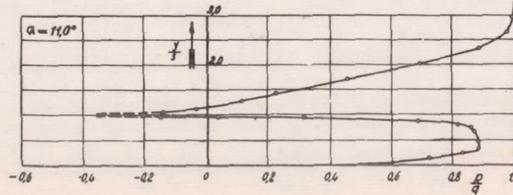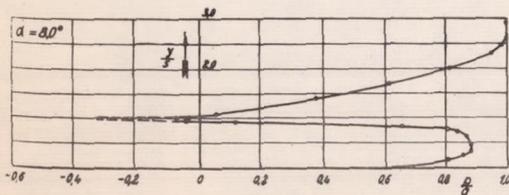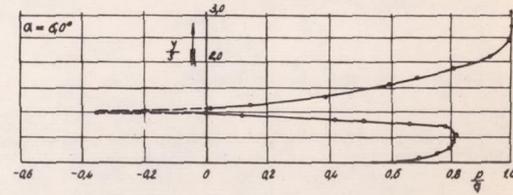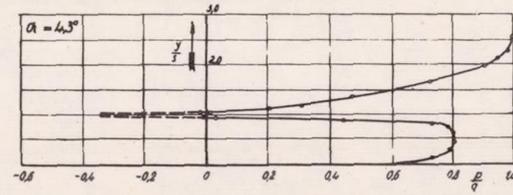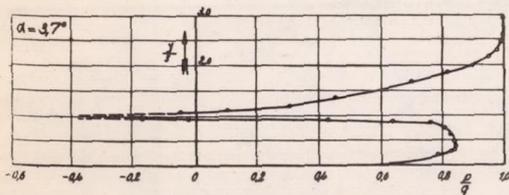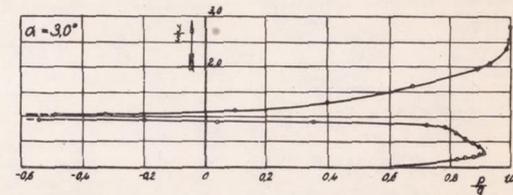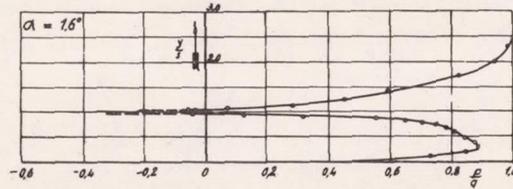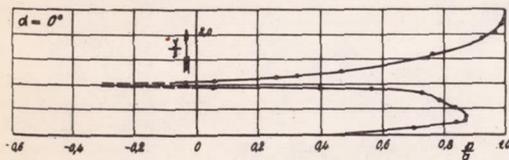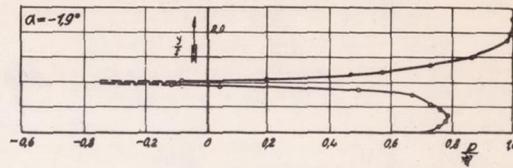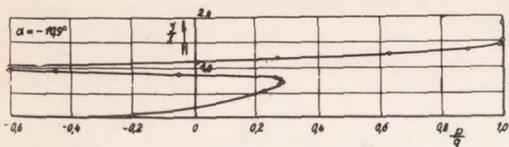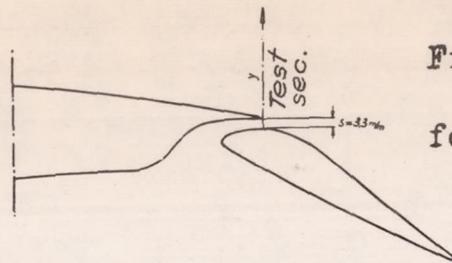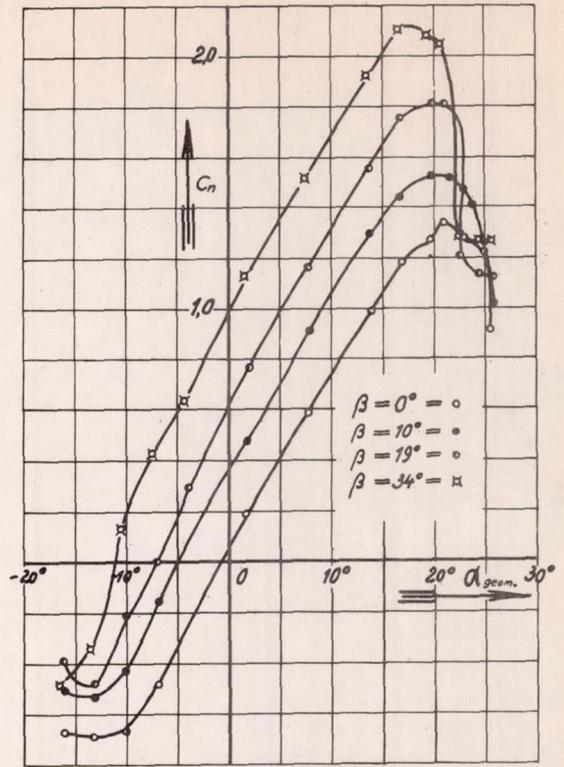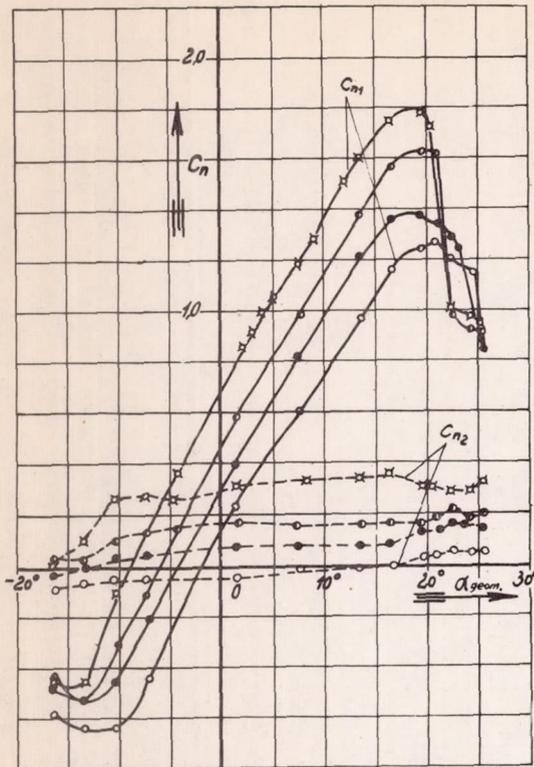
Figure 13.- Normal force coefficient as a function of angle of attack, c_n = coefficient of entire wing section, c_{n_1} = coefficient of main wing section, c_{n_2} = coefficient of flap section.
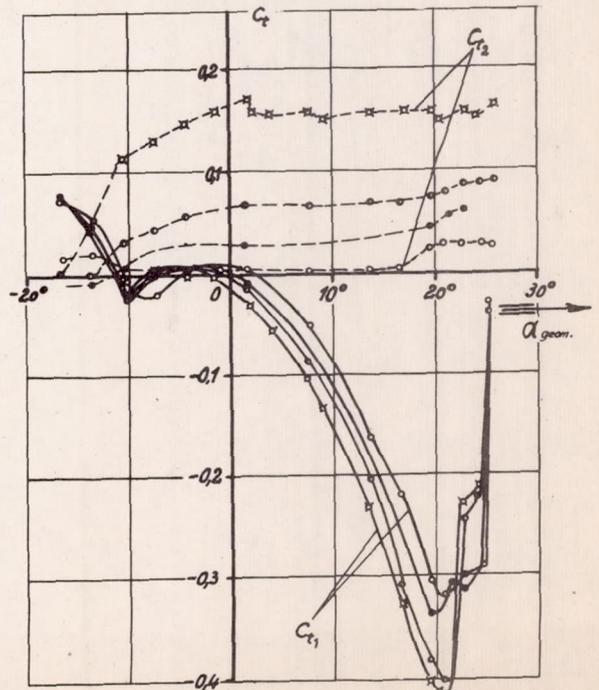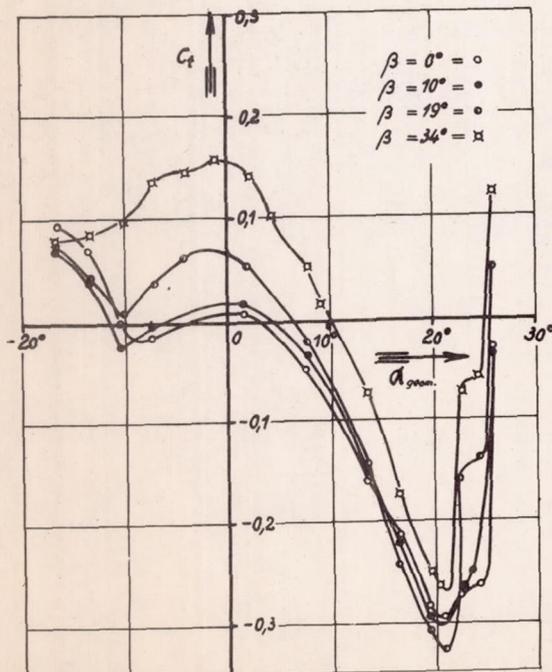

Figure 14.- Tangential force coefficient as function of angle of attack, c_t = coefficient of entire wing section, c_{t_1} = coefficient of main wing section, c_{t_2} = coefficient of flap section.
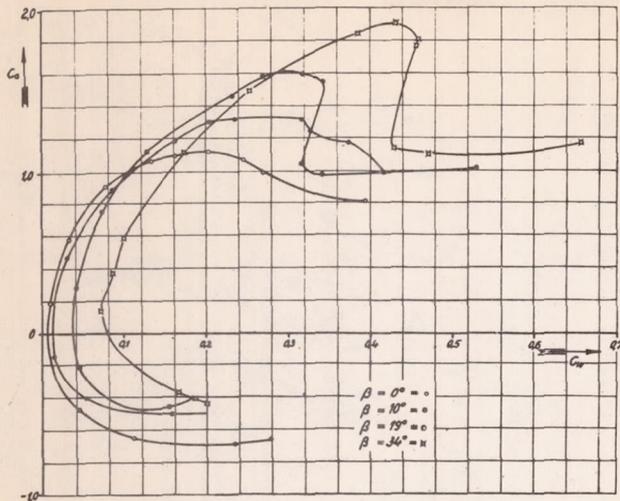
Figure 15.- Polars of investigated wing section.
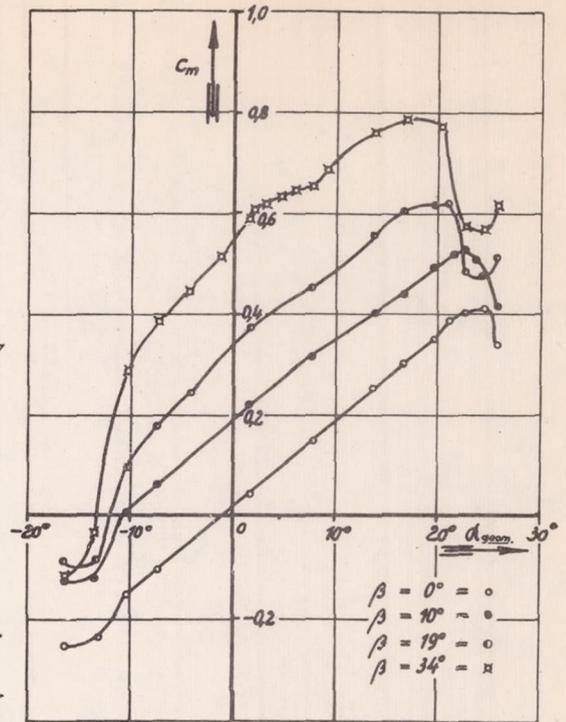
Figure 16.- Pitching moment coefficients of wing section.

Figure 20.- Comparison of maximum normal force coefficient values from the wind tunnel and flight tests.
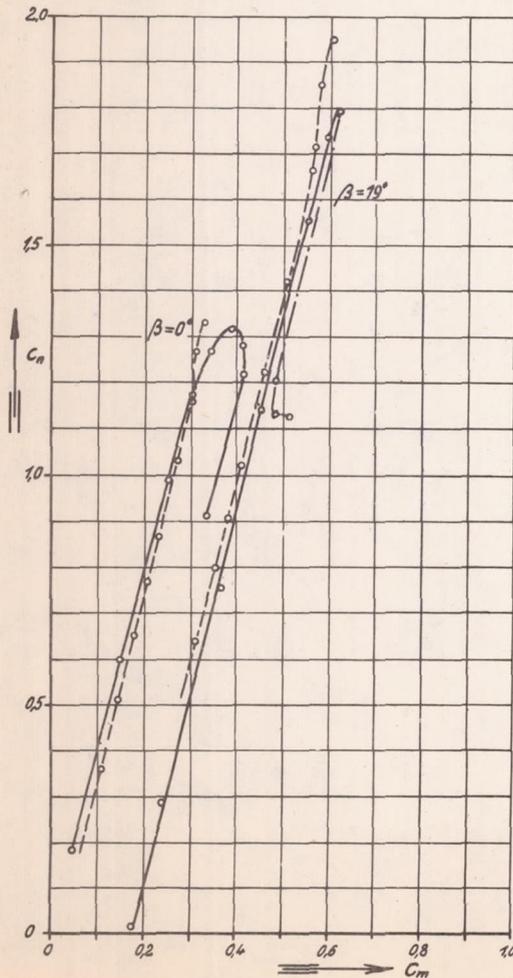
Figure 19.- Comparison of the coefficients obtained by integration of the wind tunnel and flight tests measurements. The continuous curve refers to the wind tunnel test while the dotted curve to the flight test.
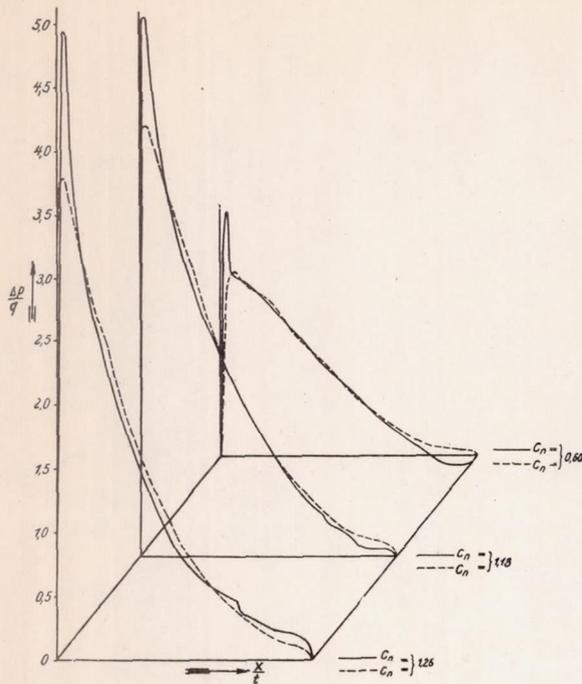
Figure 17.- Comparison of pressure
            distributions measured
in the wind tunnel at β = 0° with
the corresponding pressure distri-
butions obtained from the flight
test. The ordinates give the alge-
braic sum of the pressures on the
upper and lower surfaces. The con-
tinuous curve corresponds to the
wind tunnel test and the dotted
curve to the flight test.
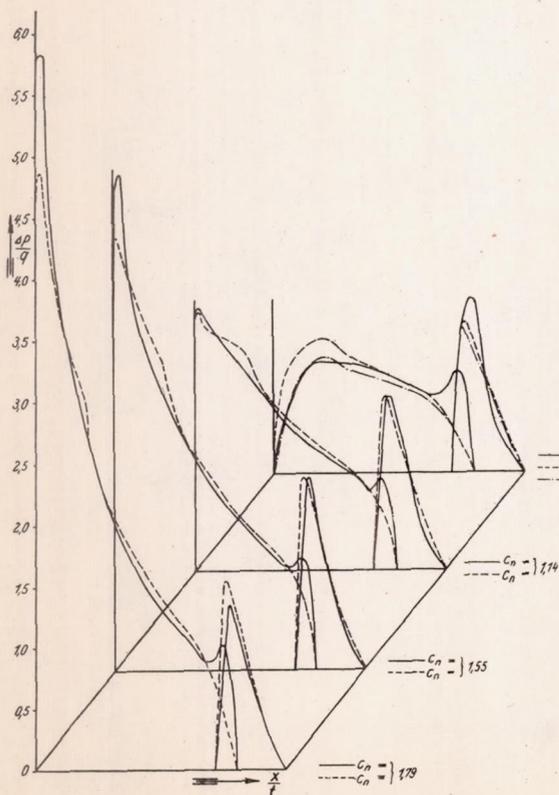
Figure 18.- Comparison of pres-
            sure distributions
measured in wind tunnel at
β=19° with the coresponding
pressure distributions obtained
from the flight test. The ordi-
nates give the algebraic sum of
the pressure on the upper and
lower surfaces. The continuous
curve coresponds to the wind
tunnel test and the dotted curve
to the flight test. The dot-
dash curve represents a pres-
sure resultant distribution for
which Kiel gives a value of
$c_n = 0.66$.